Video Article

Radio Frequency Magnetron Sputtering of $GdBa_2Cu_3O_{7-\delta}$/ $La_{0.67}Sr_{0.33}MnO_3$ Quasi-bilayer Films on $SrTiO_3$ (STO) Single-crystal Substrates

Ying Wang[1,2], Zhen Li[1,2], Yijie Li[2], Linfei Liu[2], Da Xu[2], Xiaojing Luo[1], Tian Gao[1,3], Yanyan Zhu[1,3]

[1]Department of Physics, Mathematics, Shanghai Key Laboratory of Materials Protection and Advanced Materials in Electric Power, Shanghai University of Electric Power

[2]Key Laboratory of Artificial Structure and Quantum Control, Ministry of Education, Department of Physics, Shanghai Jiao Tong University

[3]Shanghai Key Laboratory of High Temperature Superconductors, Shanghai University

Correspondence to: Ying Wang at 2006000081@shiep.edu.cn

URL: https://www.jove.com/video/58069
DOI: doi:10.3791/58069

Keywords: LSMO/ (Gd) BCO films, RF-sputtering, superconductivity, ferromagnetic, nanoparticles, quasi-bilayer film structure

Date Published: 10/19/2018

Citation: Wang, Y., Li, Z., Li, Y., Liu, L., Xu, D., Luo, X., Gao, T., Zhu, Y. Radio Frequency Magnetron Sputtering of $GdBa_2Cu_3O_{7-\delta}$/ $La_{0.67}Sr_{0.33}MnO_3$ Quasi-bilayer Films on $SrTiO_3$ (STO) Single-crystal Substrates. *J. Vis. Exp.* (), e58069, doi:10.3791/58069 (2018).

Abstract

Here, we demonstrate a method of coating ferromagnetic $La_{0.67}Sr_{0.33}MnO_3$ (LSMO) nanoparticles on (001) $SrTiO_3$ (STO) single-crystal substrates by radio frequency (RF) magnetron sputtering. LSMO nanoparticles were deposited with diameters from 10 to 20 nm and heights between 20 and 50 nm. At the same time, (Gd) $Ba_2Cu_3O_{7-\delta}$ ((Gd) BCO) films were fabricated on both undecorated and LSMO nanoparticle decorated STO substrates using RF magnetron sputtering. This report also describes the properties of $GdBa_2Cu_3O_{7-\delta}$/ $La_{0.67}Sr_{0.33}MnO_3$ quasi-bilayer films structures (*e.g.,* crystalline phase, morphology, chemical composition); magnetization, magneto-transport, and superconducting transport properties were also evaluated.

Introduction

The hole-doped manganite $La_{0.67}Sr_{0.33}MnO_3$ (LSMO) have unique properties such as wide-band gaps, half-metallic ferromagnetism, and entangled electronic states, which provide extraordinary opportunities for potential spintronic applications[1,2,3,4]. Currently, many researchers are endeavoring to take advantage of the unique properties of LSMO to inhabit the vortex movement for high temperature superconducting (HTS) films, such as (RE) $Ba_2Cu_3O_{7-\delta}$ films (REBCO, RE= rare-earth element)[5,6,7,8,9,10,11,12]. Nanoscale decoration of the substrate surfaces with ferromagnetic nanoparticles will provide well-defined sites for inducing magnetic pinning centers of expected density[13,14]. However, the ability to control the density and geometry of the nanoparticles on highly textured surfaces, such as on single-crystal substrates and highly textured metal substrates is very difficult. Most commonly, nanoparticles are synthesized and coated on surfaces using metal organic decomposition methods[15], and pulsed laser deposition methods[16,17]. Although pulse laser deposition methods can provide nanoparticles coated on various substrates, it is difficult to realize large area homogeneous nanoparticles deposition. As for metal organic decomposition methods, they are proper for large area deposition of nanoparticles. However, the nanoparticles are often non-uniform and easily damaged by small physical stresses.

Among these techniques, RF-magnetron sputtering has many advantages. Sputtering has a high deposition rate, low cost, and a lack of toxic gas emission. Also, it is easy to expand to large scale area substrates[18,19]. This method provides single-step formation of $La_{0.67}Sr_{0.33}MnO_3$ (LSMO) nanoparticles, and the nanoparticles are easy to be deposited on single-crystal substrates. RF magnetron sputtering can create large area nanoparticles uniformly on a diverse range of substrates, irrespective of surface texture, and surface roughness[20].The particle control can be achieved by adjust sputtering time. Homogeneity can be achieved by adjust target-substrate distance. The disadvantage of RF-magnetron sputtering is its lower growth rate for some oxides[21]. In this approach, target atoms (or molecules) are sputtered out of the target by argon ion, and then nanoparticles are deposited on substrates in the vapor phase[22]. Nanoparticles formation occurs on the substrate in a single step[23]. This method is theoretically applicable to any materials including superconducting thin film, resistance film, semiconductor film, ferromagnetic thin film *etc.* However, to date, reports about protocols for depositing ferromagnetic nanoparticles are very scarce.

Here, we demonstrate the deposition of $GdBa_2Cu_3O_{7-\delta}$/$La_{0.67}Sr_{0.33}MnO_3$ quasi-bilayer films on $SrTiO_3$ (STO) single-crystal substrates by RF magnetron sputtering method. Two kinds of target materials, $GdBa_2Cu_3O_{7-\delta}$ and $La_{0.67}Sr_{0.33}MnO_3$ target are used in the process. $SrTiO_3$ (STO) single-crystal substrates were coated with $GdBa_2Cu_3O_{7-\delta}$films and $GdBa_2Cu_3O_{7-\delta}$/$La_{0.67}Sr_{0.33}MnO_3$ quasi-bilayer films.

In this protocol, $GdBa_2Cu_3O_{7-\delta}$/$La_{0.67}Sr_{0.33}MnO_3$ Quasi-bilayer films are deposited with RF magnetron sputtering on STO (001) substrates. The target diameter is 60 mm and the distance between the target and substrates is about 10 cm. The heaters are bulbs positioned 1 cm above the substrates. The maximum temperature is 850°C in this system**.** There are 5 different substrates in this system. RF magnetron sputtering $GdBa_2Cu_3O_{7-\delta}$/$La_{0.67}Sr_{0.33}MnO_3$ quasi-bilayer films consists of two steps, which are the preparation of substrates and the RF magnetron sputtering process. A picture of the sputtering system is shown in **Figure S1**.

Protocol

1. Substrate and Target Preparation

NOTE: This section describes the preparation of the sputter deposition chamber and the single crystal $SrTiO_3$ (STO) substrates.

1. Use 10 mm x 10 mm $SrTiO_3$ (STO) single-crystal substrates during the RF magnetron sputtering process.
2. Sequentially clean the substrates in isopropanol and deionized water for 10 min each at room temperature in ultrasonic bath. Then dry the substrates with nitrogen, which is for uniform covering of the substrate and good film adherence.
3. Mount the (001) STO substrates in the substrate holders with silver powder conductive glue. Load these into the vacuum chamber.
4. Mount the LSMO target in the magnetron injection gun, and then reassemble the gun. Test the resistance with an ohmmeter, to avoid a short circuit between the magnetron and the surrounding shield. Close the vacuum chamber is closed and pump down.
5. Once the vacuum is lower than 1 x 10^{-4} Pa, heat the substrates to 850 °C using a heating rate of 15 °C/min. set the target-substrate distance to 8 cm.
6. Set the mass flow controller to 10 sccm of O and 5 sccm of Ar as working gas flow. Use Ar/ O mixed gas to keep O cationic ratio (3) for $La_{0.67}Sr_{0.33}MnO_3$ material during growth.
7. Before the deposition, pre-sputter the LSMO target for 20 min at 30 W. High power will lead to cracks in the target and using low power will lead to more time for a clean surface, so we choose 20 min for 30 W.

2. LSMO Nanoparticle Deposition

NOTE: This section describes the deposition of the LSMO nanoparticles by RF-magnetron sputtering.

1. To obtain a chamber pressure of 25 Pa, adjust the molecular pump splint valve. If the instant value is becoming larger than 25 Pa, rotate it counter-clockwise; if it is becoming smaller than 25Pa, rotate it clockwise. Continue until the pressure has settled to a stable value.
2. Check that the substrate temperature remains at 850 °C and is stable.
3. Increase the power of magnetron from 30 to 80 W. Wait for 10 min, until the plasma is stabilized.
4. Open the shutter and deposit LSMO on the heated substrate.
   NOTE: We used sputtering times of 5, 10, 30, and 60 s for four samples.
5. Close the shutter. Shut off power to the magnetron. Close the gas valve and shut off heater power.
6. Cool the samples to room temperature. Unusually, this takes at least two hours in this system. Vent the chamber with dry nitrogen, open it, and remove the samples.

3. $GdBa_2Cu_3O_{7-\delta}$ Film Deposition

1. Mount the $GdBa_2Cu_3O_{7-\delta}$target in the magnetron gun, then reassemble the gun. Deposit any (Gd) BCO films, using steps similar to steps 1.4-2.8. Use similar deposition conditions for (Gd) BCO films as for the LSMO nanoparticles, except for the sputtering time which should be 30 min. After this, the growth will be over, and next step is the post-annealing.
2. Decrease the sample temperature to 500°C. Then, open the gas valve for oxygen to give a chamber pressure of 75,000 Pa. Hold the samples at this temperature for one hour.
   NOTE: The temperature for 500 °C and a chamber pressure of 75, 000 Pa are for uniformly achieving LSMO nanoparticles.
3. Cool the samples to room temperature. Vent the chamber with dry nitrogen, open it, and remove the samples.

Representative Results

The thickness of (Gd) BCO films on both bare and LSMO decorated STO substrate was 500nm, which was measured by a surface profilometer. The film thickness was controlled by sputtering time. **Figure 1a,b** shows the AFM image of LSMO nanoparticle (sputtering time of 10 s) on 1.0 cm x 1.0 cm single-crystal STO substrates to prove that the LSMO nanoparticles grown on STO substrates uniformly. The surface and to measure the roughness of the films was characterized by atomic force microscopy (AFM) working in tapping Mode. The diameter of these LSMO nanoparticles ranged from 10 to 20 nm. Their height ranged from 20 to 50 nm. With an appropriate adjustment of deposited parameters, such as growth temperatures and target-substrate distance, different surface topography could be achieved, as shown in **Figure 1c,d**. At a low temperature (650 °C), particle and line mixed topography was obtained, as seen in **Figure 1c**. Furthermore, a small target-substrate distance (6 cm) can lead to a high density of LSMO particles with small size (**Figure 1d**). The structure of the LSMO nanoparticles (sputtering time of 10 s) and (Gd) BCO films (**Figure 2**) was measured by X-ray diffractometer (XRD) measurement with Cu K radiation operated at 40 kV and 20 mA. In **Figure 3**, results are shown for two representative (Gd) BCO samples as described above: (Gd) BCO films on undecorated and LSMO decorated substrates. The superconducting transition temperature (Tc) was close to 90.5 K for pure GBCO film and 90.3 K for LSMO/GBCO films. This nearly equal Tc value indicates LSMO nanoparticles don't harm the superconducting property (Tc) for (Gd) BCO films. The higher slope indicate smaller Tc width for pure GBCO film compared with LSMO/GBCO films. The magnetization hysteresis loops for these two samples are plotted in **Figure 4**. By comparison, the M-H loop area is much bigger from 0 to 6 T at 30K for (Gd) BCO films fabricated on LSMO decorated substrate. The same trend is found at 50 and 77 K.

Representative J-H distributions are also shown for each sample in **Figure 5**. For a given magnetic field, these distributions are calculated as

$$J_c = 2\Delta M \times \left[a\left(1 - \frac{a}{3b}\right)\right]^{-1}$$

where a and b are the length and width of the tested sample. A magnetic field, which is perpendicular to the sample plane, a < b, is applied during testing process. In our case, a and b are 3 mm and 4 mm, respectively. The ΔM symbols in the formula is the difference between upper and lower values of a magnetic hysteresis loop at the same H, as shown in **Figure 4**. The critical current density and its dependences of field help will give more information for the effect of LSMO nanoparticles on flux pinning properties. These data in **Figure 5a** suggest that the (Gd) BCO film deposited on LSMO decorated substrate possess a higher Jc value from 1.3 to 6 T at 30 K. Furthermore, as shown in **Figure 5b**, the (Gd) BCO film fabricated on LSMO decorated substrate shows a higher Jc value from 0 to 6 T at 77 K. The two phenomena in **Figure 5** suggests that an additional pinning mechanism exist in (Gd) BCO films on LSMO decorated substrates. We named it as magnetic pinning, which is due to LSMO nanoparticles deposited on the substrate.

The pinning force density was calculated by Fp = Jc × B. The calculated result is shown in **Figure 6a,b**. There is a crossing point at 1.3T for Fp (max) value at 30K (**Figure 6a**), above which, the decorated sample has larger Fp value. The Fp (max) value at 77K moved to a higher H value (from 0.6 T to 2.5 T) for sample with decoration, which is shown in **Figure 6b**. This difference also indicates there are different pinning mechanisms for (Gd) BCO film with and without LSMO decoration.

We measured the critical current density dependence on magnetic field orientation for obtaining further interesting information on the vortex pinning properties. **Figure 7** shows the angular dependence of Jc at 0.3T and 77 K for (Gd) BCO film with and without LSMO decoration. It is found that the most prominent increase of Jc is along the c-axis. This suggests that it is more effective at a field orientation of H//c for LSMO decorated (Gd) BCO film. For explaining the phenomenon, we show a schematic in the inset of **Figure 7**, which shows threading dislocations generated at H//c direction. We believe that the threading dislocations along the c-axis in a (Gd) BCO film with LSMO decoration is responsible for this phenomenon.

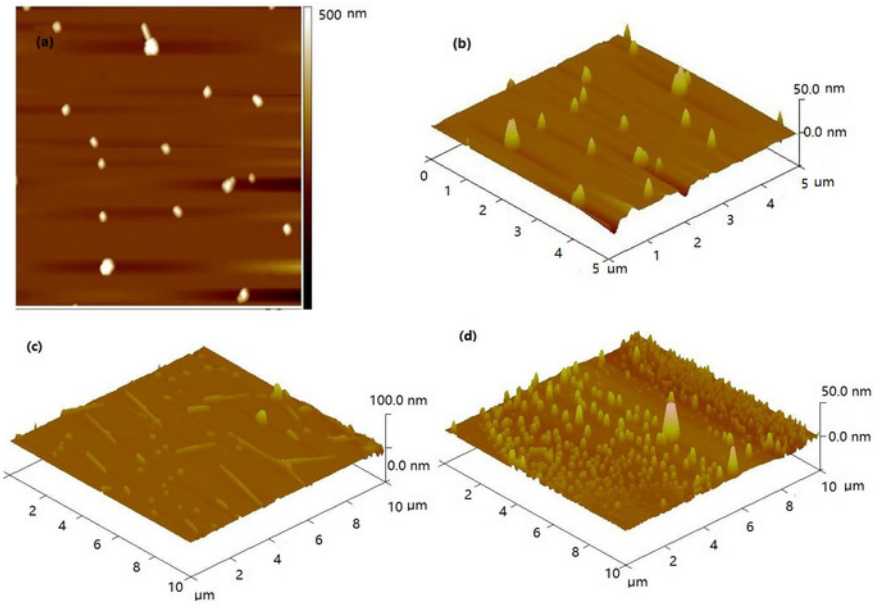

Figure 1: Atomic Force Microscopic image of LSMO nanoparticle decorated STO substrates. (a) 2D image, (b) 3D image, (c) 3D image of sample grown at a low temperature (650 °C), and (d) 3D image of sample grown at a small target-substrate distance (6 cm). Reprinted with permission from previous work[12]. Copyright 2018 Elsevier. Please click here to view a larger version of this figure.

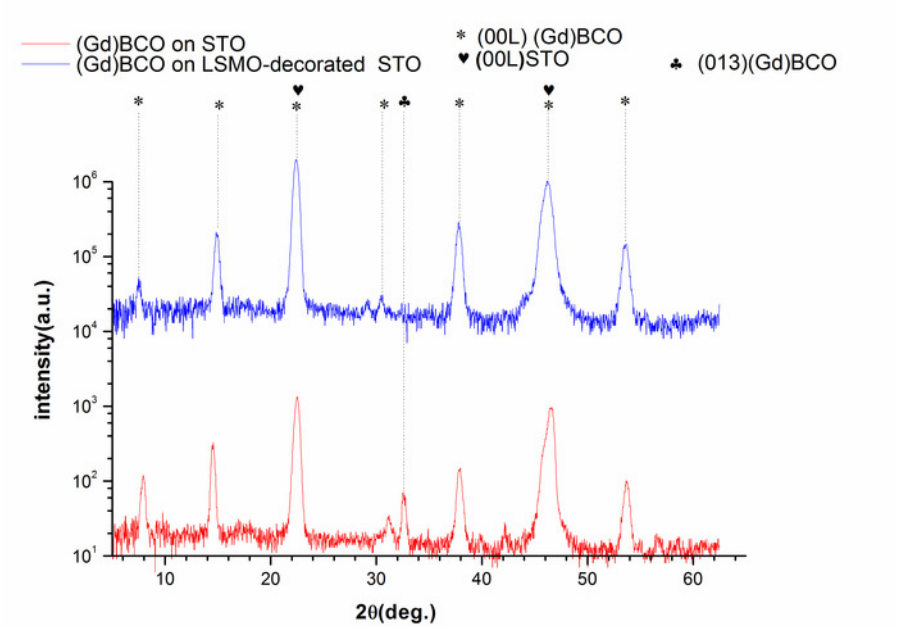

Figure 2: XRD pattern of (Gd) BCO thin films fabricated on undecorated and LSMO nanoparticle decorated STO substrates. Reprinted with permission from previous work[12]. Copyright 2018 Elsevier. Please click here to view a larger version of this figure.

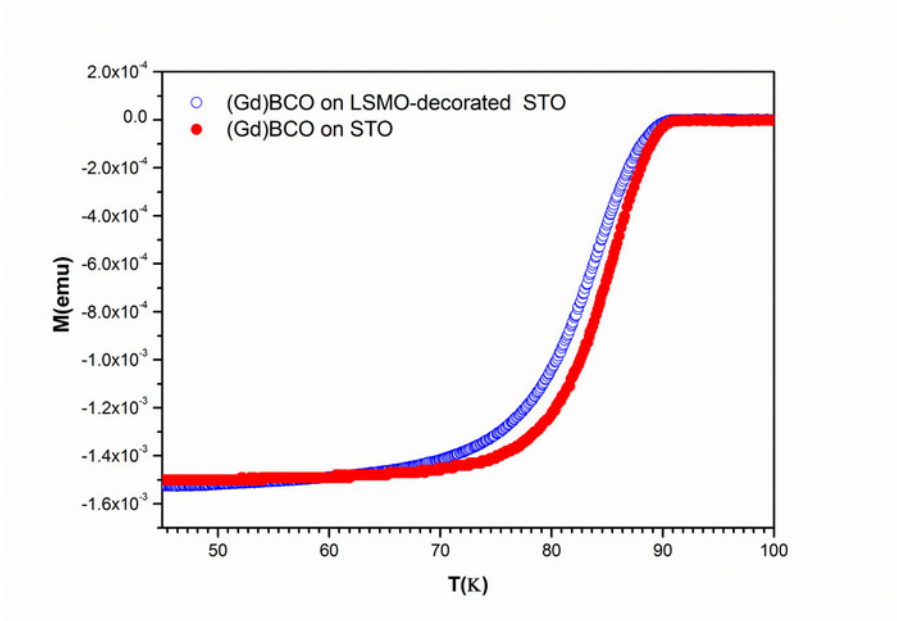

Figure 3: DC magnetization measurements of the superconducting transition Tc for (Gd) BCO thin films fabricated on undecorated and LSMO nanoparticle decorated STO substrates. Reprinted with permission from previous work[12]. Copyright 2018 Elsevier. Please click here to view a larger version of this figure.

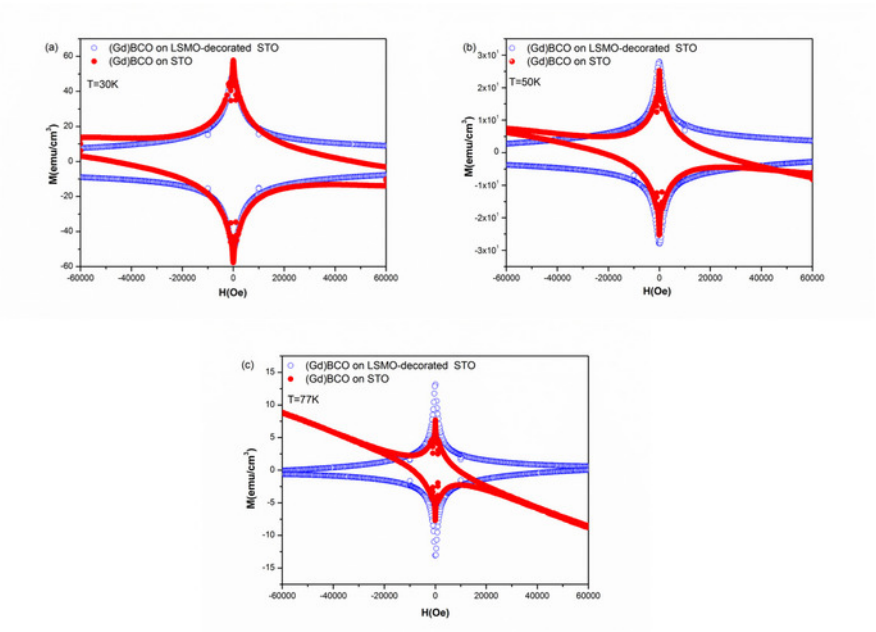

Figure 4: Magnetization hysteresis loops for (Gd) BCO thin films on the undecorated and LSMO nanoparticle decorated STO substrates at three different temperatures. (a) 30 K, **(b)** 50 K, and **(c) 77 K.** Reprinted with permission from previous work[12]. Copyright 2018 Elsevier. Please click here to view a larger version of this figure.

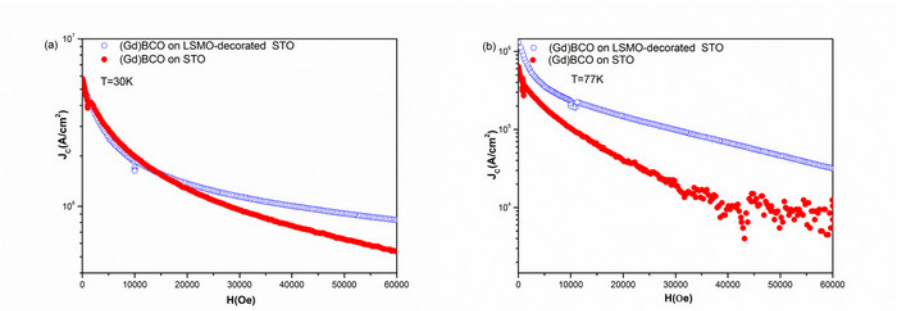

Figure 5: Field dependence of Jc (the critical current density) for (Gd) BCO thin films on undecorated and LSMO decorated STO substrates at (a) 30 K and (b) 77 K. Reprinted with permission from previous work[12]. Copyright 2018 Elsevier. Please click here to view a larger version of this figure.

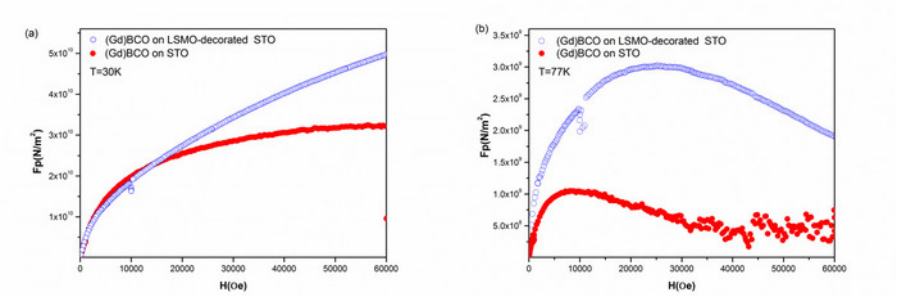

Figure 6: Variation of Fp as a function of the applied magnetic field for (Gd)BCO films deposited on undecorated and LSMO-nanoparticle-decorated STO substrates. (**a**) 30 K and (**b**) 77 K. Reprinted with permission from previous work[12]. Copyright 2018 Elsevier. Please click here to view a larger version of this figure.

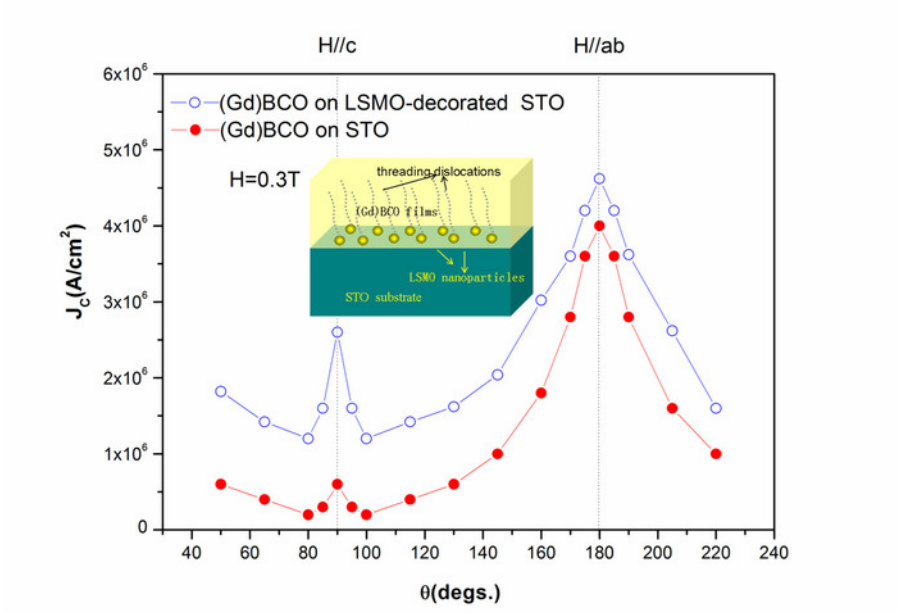

Figure 7: Dependence of Jc at 0.3 T and 77 K on orientation of the applied magnetic field, relative to the film's normal direction. The inset shows the schematic diagram of threading dislocations generated along the c-axis in the LSMO decorated (Gd) BCO thin film. Reprinted with permission from previous work[12]. Copyright 2018 Elsevier. Please click here to view a larger version of this figure.

Figure S1: Picture of the RF sputtering system. Please click here to view a larger version of this figure.

Discussion

Here we have demonstrated that this method can be used to prepare LSMO ferromagnetic nanoparticles of uniform distribution on $SrTiO_3$ (STO) single-crystal substrates. The (Gd) BCO films also can be deposited on both bare and LSMO decorated STO substrate. With an appropriate adjustment of deposited parameters, such as growth temperatures and target-substrate distance, this method ought to be useful for deposited different kinds of magnetic and non-magnetic particles or layers, for example, CeO_2, YSZ (yttrium-stabilized zirconia)[24], and ITO (Indium tin oxide).

A critical step in the protocol is the sputtering time for deposition of LSMO particles. In the protocol, the proper sputtering time is needed. If the sputtering time is too long, this will form continuous LSMO thin film not nanoparticles. On the other hand, if the sputtering time is too short, the density of LSMO nanoparticles is not enough and it will affect current carrying ability for top GBCO films. For GBCO films, in order to achieve epitaxy, the use of a single crystal substrate is needed. In our case, LSMO nanoparticles do not need to achieve epitaxy, but just need greater

density and the proper size to enhance top GBCO superconducting properties. In this report, sputtering times are used to control the different morphology for LSMO nanoparticles.

One drawback of our deposition chamber is that because there is no *in situ* QCM (quartz crystal microbalance) sensor, we cannot monitor in real time the film thickness and deposition during the growth process. In our case, the thickness of GBCO films can be controlled by sputtering times. The deposition rate of the GBCO films presented here is about 15 nm/min. Finally, as mentioned in the introduction, the fabrication of LSMO nanoparticles has been successfully achieved by either metal organic decomposition methods (MOD) or pulsed laser deposition methods (PLD). The PLD method possesses slower deposition rates and involves a larger investment, while the MOD method results uniform particle distribution and low reproduction. Concerning the RF sputtering deposition, it can provide particles with uniform distribution and lower investment with respect to PLD method. Also, this nanoparticle deposition procedure can be scaled-up to coat larger surfaces easily.

In conclusion, we demonstrate a RF sputtering method with which to create ferromagnetic LSMO nanoparticles on STO substrate, and GBCO superconducting films on bare and LSMO decorated STO substrate. These ferromagnetic LSMO nanoparticles have never been synthesized by RF sputtering deposition before. This RF sputtering method can coat nanoparticles uniformly on $SrTiO_3$ (STO) single-crystal substrates or high textured substrates with different particle density and size[17,25]. This feature allows for future application of RF sputtering ferromagnetic nanoparticles in electronics devices on single-crystal substrates or flexible and highly textured substrates.

Disclosures

The authors have nothing to disclose.

Acknowledgements

This work was supported by the National Natural Science Foundation of China (No. 51502168; No.11504227) and the Shanghai Municipal Natural Science Foundation (No.16ZR1413600).The authors gratefully thank the Instrumental Analysis Center of Shanghai Jiao Tong University and Ma-tek analytical lab for competent technical assistance.

References

1. Gong, J., Zheng, D., Li, D., Jin, C., & Bai, H. Lattice distortion modified anisotropic magnetoresistance in epitaxial La0.67Sr0.33MnO3 thin films. *Journal of Alloys and Compounds.* **735**, 1152-1157 (2018).
2. Wang, J., Han, Z., Bai, J., Luo, B., & Chen, C. Magnetoelectric coupling in oxygen deficient La0.67Sr0.33MnO3-δ/BaTiO3 composite film. *Physica B: Condensed Matter.* **534**, 141-144 (2018).
3. Duan, Z. *et al.* Facile fabrication of micro-patterned LSMO films with unchanged magnetic properties by photosensitive sol-gel method on LaAlO3 substrates. *Ceramics International.* **42** (12), 14100-14106 (2016).
4. Xu, P., Huffman, T. J., Kwak, I. H., Biswas, A., & Qazilbash, M. M. Temperature dependent infrared nano-imaging of La0.67Sr0.33MnO3 thin film. *Journal of Physics-Condensed Matter.* **30** (2) (2018).
5. Bulaevskii, L. N., Chudnovsky, E. M., & Maley, M. P. Magnetic pinning in superconductor-ferromagnet multilayers. *Applied Physics Letters.* **76** (18), 2594-2596 (2000).
6. Chen, C. Z. *et al.* Flux pinning of stress-induced magnetic inhomogeneity in the bilayers of YBa2Cu3O7−δ/La0.67Sr0.33MnO3−δ. *Journal of Applied Physics.* **106** (9), 093902 (2009).
7. Chen, C. Z. *et al.* Robust high-temperature magnetic pinning induced by proximity in YBa2Cu3O7−δ/La0.67Sr0.33MnO3 hybrids. *Journal of Applied Physics.* **109** (7), 073921, (2011).
8. Huang, J. *et al.* Magnetic properties of (CoFe2O4)x:(CeO2)1−x vertically aligned nanocomposites and their pinning properties in YBa2Cu3O7−δ thin films. *Journal of Applied Physics.* **115** (12), 123902, (2014).
9. Lange, M., Bael, M. J. V., Bruynseraede, Y., & Moshchalkov, V. V. Nanoengineered Magnetic-Field-Induced Superconductivity. *Physical Review Letters.* **90** (19), 197006 (2003).
10. Rakshit, R. K., Budhani, R. C., Bhuvana, T., Kulkarni, V. N., & Kulkarni, G. U. Inhomogeneous vortex-state-driven enhancement of superconductivity in nanoengineered ferromagnet-superconductor heterostructures. *Physical Review B.* **77** (5), 052509 (2008).
11. Guo, H., & Ward, T. Z. Fabrication of Spatially Confined Complex Oxides. *Journal of Visualized Experiments.* **77**, e50573 (2013).
12. Wang, Y., Li, Y., Liu, L., & Xu, D. Improvement of flux pinning in GdBa2Cu3O7-delta thin film by nanoscale ferromagnetic La0.67Sr0.33MnO3 pretreatment of substrate surface. *Ceramics International.* **44** (1), 225-230 (2018).
13. Martín, J. I., Vélez, M., Nogués, J., & Schuller, I. K. Flux Pinning in a Superconductor by an Array of Submicrometer Magnetic Dots. *Physical Review Letters.* **79** (10), 1929-1932 (1997).
14. Morgan, D. J., & Ketterson, J. B. Asymmetric Flux Pinning in a Regular Array of Magnetic Dipoles. *Physical Review Letters.* **80** (16), 3614-3617 (1998).
15. Gutierrez, J. *et al.* Anisotropic c-axis pinning in interfacial self-assembled nanostructured trifluoracetate-YBa2Cu3O7−x films. *Applied Physics Letters.* **94** (17), 172513 (2009).
16. Tran, D. H. *et al.* Enhanced critical current density in GdBa2Cu3O7-δ thin films with substrate surface decoration using Gd2O3 nanoparticles. *Thin Solid Films.* **526** (0), 241-245 (2012).
17. Jha, A. K., Khare, N., & Pinto, R. Interface engineering using ferromagnetic nanoparticles for enhancing pinning in YBa2Cu3O7-delta thin film. *Journal of Applied Physics.* **110** (11) (2011).
18. Casotti, D. *et al.* Ageing effects on electrical resistivity of Nb-doped TiO2 thin films deposited at a high rate by reactive DC magnetron sputtering. *Applied Surface Science.* **455**, 267-275 (2018).
19. Li, Y. *et al.* Preparation of single-phase Ti2AlN coating by magnetron sputtering with cost-efficient hot-pressed Ti-Al-N targets. *Ceramics International.* **44** (14), 17530-17534 (2018).

20. Mahdhi, H., Djessas, K., & Ben Ayadi, Z. Synthesis and characteristics of Ca-doped ZnO thin films by rf magnetron sputtering at low temperature. *Materials Letters.* **214**, 10-14 (2018).
21. Shen, H., Wei, B., Zhang, D., Qi, Z., & Wang, Z. Magnetron sputtered NbN thin film electrodes for supercapacitors. *Materials Letters.* **229**, 17-20 (2018).
22. Sinnarasa, I. *et al.* Influence of thickness and microstructure on thermoelectric properties of Mg-doped CuCrO2 delafossite thin films deposited by RF-magnetron sputtering. *Applied Surface Science.* **455**, 244-250 (2018).
23. Thi-Thuy-Nga, N., Chen, Y.-H., Chen, Z.-M., Cheng, K.-B., & He, J.-L. Microstructure, near infrared reflectance, and surface temperature of Ti-O coated polyethylene terephthalate fabrics prepared by roll-to-roll high power impulse magnetron sputtering system. *Thin Solid Films.* **663**, 1-8 (2018).
24. Wang, Y., Xu, D., Li, Y., & Liu, L. Texture and morphology developments of Yttria-stabilized zirconia (YSZ) buffer layer for coated conductors by RF sputtering. *Surface & Coatings Technology.* **232**, 497-503 (2013).
25. Petrisor, T., Jr. *et al.* Magnetic pinning effects of epitaxial LaxSr1-xMnO3 nanostructured thin films on YBa2Cu3O7-delta layers. *Journal of Applied Physics.* **112** (5), 053919-1-053919-7 (2012).

